Mapping structurally favourable zones of water seepage using remote sensing and geophysical methods in western Rajasthan, India

Abstract

Birendra Pratap

Department of Geophysics, Institute of Science, Banaras Hindu University, Varanasi 221005 U.P. India

Corresponding author: bpratap@bhu.ac.in

IRCID: 0000-0002-7059-4516

Author Contributions The author contributed to the study's conception and design. Material preparation, data collection and interpretation.

The presence of cracks, joints, faults, fractures, and lineaments and their interconnectivity influence the water movement in hard rock areas. The groundwater level in Jodhpur city, western Rajasthan, has been rising significantly over the past few years, and this has attracted attention due to the region's unfavourable impacts. In many parts of the city, particularly around popular markets, water levels have touched the ground. The rise in groundwater levels has caused water seepage in the basements of underground shops and houses throughout the city. Traditional field survey techniques require a lot of money and effort to map water seepage zones. In this study, subsurface signatures of linear features, faults, and fractures were quickly and inexpensively mapped using a remote sensing methodology. Fracture zones that are prone to water seepage were identified using an electrical resistivity method. Based on meticulous analysis of satellite imagery, a number of minor and large lineament sets have been mapped, the majority of which cross over Kailana Lake-Takht Sagar and enter the city. According to the study of all available data, fractured zones exist, are linked by Kailana Lake-Takht Sagar, and act as conduits for water seepage. The presence of obvious lineaments also facilitates water seepage.

Keywords: Cross-section, Fracture zone, Groundwater, Lineaments, Seepage

1. Introduction

The application of remote sensing technology is particularly effective for the resolution of groundwater problems due to the synoptic, repetitive, multi-spectral coverage of a terrain and the systematic delineation of

distinct geomorphological units (Sahai et al., 1991; Isiortho and Nkereuwem, 1996; Mulder et al., 2011). Depending on the geographical resolution, the synoptic coverage aids in the local and regional delineation of lithological, geomorphological, and structural elements. Such information is essential for planning and carrying out projects to address groundwater issues, particularly in inaccessible and hard-rock terrain. In addition, the integration of remote sensing techniques and field investigation has contributed to enhancing the mapping of geological and structural features (Mshiu, 2011; Tagnon et al., 2018; Hamimi et al., 2020). However, in recent years, initiatives for the management and development of water resources, surface hydrology, and hydrogeology have all benefited significantly from the usage of remote sensing techniques (Rao 2000). Numerous researchers have reported using GIS and remote sensing to solve groundwater problems like delineating and mapping groundwater potential zones (Dar et al., 2010; Machiwal et al., 2011; Suganthi et al., 2013; Manap et al., 2014; Elbeih, 2014; Shekhar and Pandey, 2015; Nejad et al., 2017; Mageshkumar et al., 2019; Raju et al., 2019; Bera et al., 2020; Bhattacharya 2020; Al-Djazouli et al., 2020). In hydrogeological research, the integrated use of geophysical and remote sensing techniques has been extensively outlined by various researchers (Denne et al., 1984; Singh and Prakash, 2002; Rai et al., 2005; Srivastava and Bhattaycharya, 2006; Srivastava et al., 2012; Sharafi and Khazaei, 2013; Elmahdi and Mohamed, 2014; Dailey et al., 2015).

The majority of groundwater circulation occurs in hard rock areas because of secondary porosity, which is developed by faulting, fracturing, and lineament junction of the underlying rocks (Ali et al., 2012; Das, 2017; Bera et al., 2020). Water seepage is the most prevalent hydrogeological hazard for lakes and dams, especially those located over faulted and deformed structures (Al-Fares, 2011, 2014; Yadav and Pratap, 2015; Olasunkanmi et al., 2018; Al-Fares, 2019). Multi-temporal remote sensing data provides a powerful tool to detect and delineate water seepage by lakes or water loss in transportation through canal leakage (Chopra, 1989; Engelbert et al., 1997; Huang et al., 2009; Pratap et al., 2014;). The groundwater flow was estimated using the water budget equation for Mariout Lake, Alexandria City, Egypt (Kansoh et al., 2020). The groundwater flow pattern in the western Sand Hills of Nebraska was identified using the Landsat-7 ETM (Enhanced Thematic Mapper) image. (Tcheropanov and Zolatrik, 2002). The use of remote sensing to detect seepage from irrigation canals and the visual interpretation of satellite images reveal the locations of confirmed seepage (Huang et al., 2009). Also, the high local groundwater inflow to Nosoud tunnel has been detected using satellite imagery data (Sharafi and Khazaei, 2013). The use of remote sensing to clarify the function of lineament characteristics in subterranean hydrodynamics that regulate groundwater circulation and storage (Takorabt et al., 2018). Remote

sensing methods have been used to extract lineament characteristics, namely faults and joints, from the Atalla Shear Zone and its surroundings in Egypt's Central Eastern Desert (Hamimi et al., 2020). The data from observation wells, numerical modelling, and geophysical surveys were used to create a framework for understanding seepage at the Hidden Dam site near Raymond, California (Minsley et al., 2011). A groundwater seepage study was conducted using an electrical resistivity survey to investigate the potential groundwater seepage zones (Abidin et al., 2015; Kumar et al., 2021; Guo et. al., 2022).

The groundwater movement and occurrence in the Thar Desert of western Rajasthan, India, were studied using the remote sensing data to trace the paleochannels of the legendary river Sarasvathi Drishadvati and correlate older stream channels (Ghose 1965; Ghose and Singh, 1975; Shankarnarayan et al., 1983; Kar and Ghosh, 1984; Kar 1986). The remote sensing data is used to characterise groundwater prospecting zones and delineate the role of lineaments for the assessment of groundwater in a basaltic terrain in western Rajasthan (Khan and Mohrana, 2002; Bahuguna et al., 2003; Rajput et al., 2006; Javed and Wani, 2009). Remote sensing, GIS, and modelling techniques were used to study the influence of the effluent on groundwater in Pali City, western Rajasthan (Pathak et al., 2012). Chandrasekharan (1988) conducted the geoelectrical resistivity surveys for groundwater in western Rajasthan. Geoelectrical soundings were carried out by Shukla and Pandey (1991) to determine the best location for the development of a subsurface dyke to recharge the area, close to Jodhpur city. In the Jalore district of Rajasthan, Yadav and Abolfazli (1998) used geoelectrical sounding techniques with Schlumberger configuration to demonstrate the correlation between geoelectrical features and hydraulic parameters. Yadav et al. (2000) used geoelectrical sounding in the Jhanwar region of Rajasthan and Jodhpur district to identify the presence of potential zones of fresh groundwater.

The manuscript describes remote sensing and cost effective geophysical approach to solve the adverse problem reported in the arid region in the Jodhpur City, Rajasthan India. The groundwater level has been rising in the city and covered 40% of the land area in the city. Due to rise of groundwater level, causing seepage in underground of shops and houses in the city areas and weakening the foundations and reducing the lives of the buildings and erosion take places. Keeping in view the above mentioned ground water problem. Therefore, extremely pertinent to scientifically make an assessment of favourable fractured zones of water seepage. The remote sensing technique was used to identify the surface features such as lineaments and its ground truth verification by the use of geoelectrical method. The integrated remote sensing and geoelectrical methods have

been proven a very successful in the detection of water seepage zone in the study area. The reason is that because the existing old geophysical technique use with remote sensing to solve the new problem.

In the present study, subsurface signatures of linear features, faults, and fractures were mapped using a remote sensing methodology, and fracture zones that were favourable for water seepage were identified using an electrical resistivity method. On the basis of the layer parameters obtained from the geoelectrical sounding interpretation geoelectrical cross-sections have been prepared in different directions. These cross-sections provide the clear picture of the subsurface geological formations which help in delineating the probable zone of water seepage, weathered and fractured zones occurring at different depths in the study area.

2. Geology and location of study area

According to geological data, the study region is primarily composed of sedimentary rocks and a small portion of the rhyolite suite (Blanford, 1877; Paliwal, 1992; Paliwal and Rathore, 2000). The city of Jodhpur has a typical metropolitan backdrop and an unusual geomorphological environment. The historic walled city portion is situated on the lower slope of Fort Hill Ridge. In the S-E and S-W directions, the land eventually changes to plain alluvial terrain. A series of flat-topped hills with NE-SW inclinations of rhyolite, sandstone, and shales constitute the research area. Rhyolite hills have a rough surface and an irregular relief, whereas sandstone/shale hills have an erosionally flat top. A few metres of capped sandstone can be seen on some of the rhyolite hills, showing a clear relationship between the contrasting rock formations of the two types. The Jodhpur group of sandstones and the Malani suite of igneous rocks make up the bedrock geology of the urban region. These rocks range in age from the Upper Proterozoic to the Lower Palaeozoic. Shale is interlayered with geological formations like the Malani rhyolite and Jodhpur sandstones in the city of Jodhpur. Due to the rhyolites extensive faulting, folding, weathering, and fractures, the upper layer of the rock has become extremely porous. The city, which is located on the eastern side of Kailan Lake-Takht Sagar, is primarily made up of alluvium and rhyolite geological formations. Rhyolite that is heavily faulted, worn, and fractured underlies the Kailan Lake-Takht Sagar (Sinha et al., 2002; Chandrasekharan and Navada, 2002). The Jodhpur sandstone and shale make up the largest portion of an ancient walled city. Sandstone and shale are severely deformed as a result of the neotectonic activity in the region. Significant hydrogeological formations in the study region include Jodhpur sandstone, Malani rhyolite, and quaternary alluvium. When the local water table is high, groundwater is present.

Groundwater flow, dispersion, and circulation are greatly influenced by sets of diverse joints, fractures, faults, beds of ash, and clayey minerals in the research area.

The research region, which includes parts of Jodhpur City and its surrounding area, is located in Western Rajasthan, between the latitudes of 26^0 13' N and 26^0 20' N and the longitudes of 72^0 56' E and 73^0 04' E. Jodhpur is the second-largest city in Rajasthan and was established on May 12, 1459, by the late Rao Jodhaji. It has a long history of water management. Numerous traditional water storage facilities, including jhalaras, ponds, baories (step wells), open wells, etc., can be found around the city. The Kailana Lake-Takhat Sagar are the main reservoirs for the water supply and are well connected to each other. The initial purpose of this reservoir was to store rainwater for the supply of drinking water. Numerous water supply plans have been put in place to fulfil the rising demand for water supply as the city continues to expand due to multifold development, population growth and urbanisation. The water supply needs cannot be satisfied with the available surface water and groundwater resources. The Rajiv Gandhi Lift Canal (RGLC), which additionally connects to Kailana-Takht Sagar and continuously distributes water into this reservoir to meet the rising water requirements of the city. To fulfil the increasing demand for water, it is necessary to store more water and continually improve the water level in Kailana-Takht Sagar. Unexpected circumstances have led to rising water levels in some areas of the city as well as water seepage in the basements of bustling marketplaces and underground retail establishments. Houses in these places consequently struggle with moist walls, which weaken the foundations of homes and shorten the lifespan of the structures (Gupta et al., 2007). According to a previous study, the rising water level of Kailana Lake-Takht Sagar is the cause of groundwater seepage in the city. (Sinha et al., 2002; Jigyasa, 2011; Yadav and Pratap, 2015; Kaur and Ramanathan, 2016; Pratap and Yadav, 2016). To identify favourable zones for water seepage and outline the fractured zones that operate as conduits for water seepage in the research area, accurate, quick, and cost-effective investigations are applied in the affected area.

3. Methodology

The present study used the Geographical Information System (GIS) and ERDAS-Imaging 8.6 software for satellite image processing. The methodology followed in the present study is illustrated in Fig. 1. Thematic maps, such as lineaments and relief maps, were delineated using remote sensing data from Landsat-7 ETM (Enhanced Thematic Mapper) and Survey of India topo sheets Nos. 45F/3, 45F/4, 45B/15, and 45B/16 (Das,

2017). The data used for the mapping of structural lineaments was standard and multi-date coverage (Ali et al., 2012; Takorabt et al., 2018; Tcheropanov and Zolatrik, 2002). Apart from the remote sensing data, field surveys and relevant data were also collected from secondary sources. By visually interpreting the satellite imagery, thematic maps of the research area, including lineament and relief maps, were created. Thematic maps use pictures and terrain components to identify and delineate distinct units (Rao, 1995). The data obtained by remote sensing were cross-checked by geoelectrical techniques at a few selected sites.

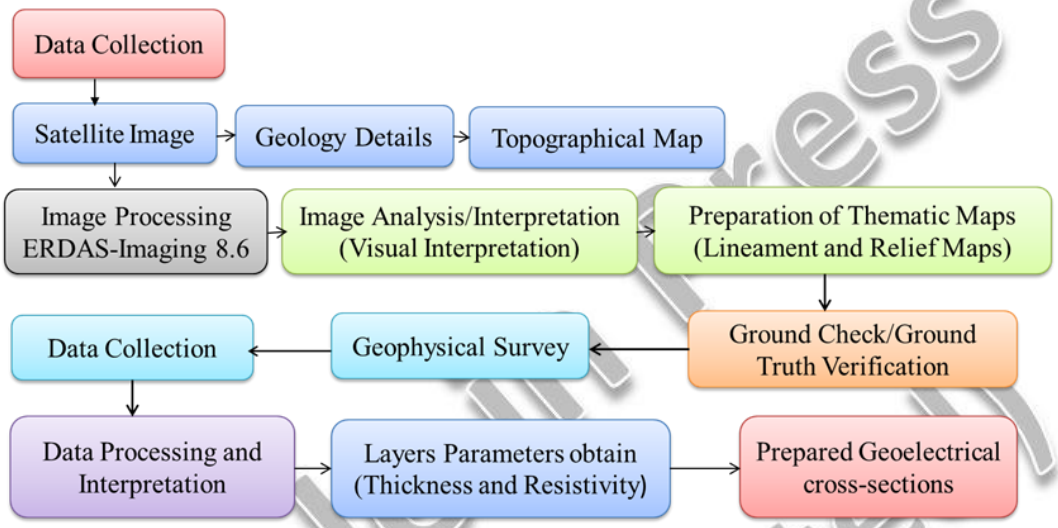

Figure 1. Flowchart showing the methodology used in the present study

The Terrameter SAS 300 resistivity meter and its accessories, made by M/s. ABEM Sweden, were utilized to collect the geoelectrical sounding data points using the Schlumberger configuration. Due to the weakening of the resistivity meter readings at each step of the current electrode spacing, the field data was collected in segments that overlapped. As a result, the potential electrode spacing was raised, and two measurements of the same current electrode spacing were made: one for the old potential electrode spacing and the other for the raised potential electrode spacing. A total of 71 geoelectrical soundings, some recent and some older, were used. For those locations where sounding data could not be taken due to field restrictions, the Ground Water Department, Jodhpur, provided the old-sounding data. Fig. 2 shows the location of these geoelectric sounding points.

On the log-log paper, the apparent resistivity values were plotted versus the half-current electrode spacing. There were two ways to interpret the field curves. First, by manually comparing the field curves to the master

curves of the Rijkswaterstaat (1969) and the associated auxiliary point charts (Ebert, 1943). Second, a software was used to interpret and correlate the data. This interpretation reveals the resistivity and thickness of each layer. The available borehole lithology has been linked to the layer characteristics of geoelectrical soundings.

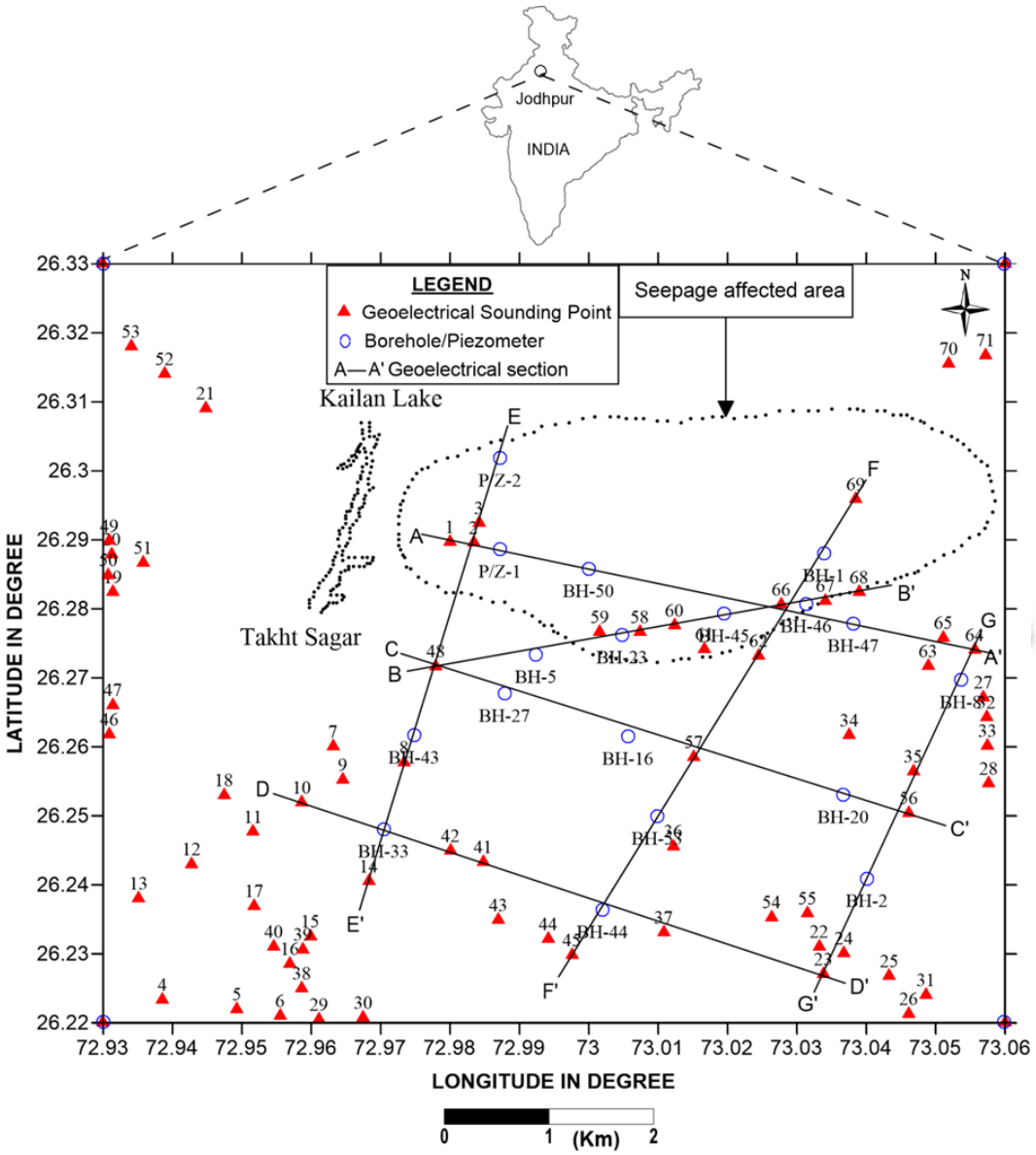

Figure 2. Study area showing geoelectrical sounding measurement

4. Results and discussion

4.1 Lineament Map

A lineament is defined as a regional large scale linear or curvilinear feature, pattern or changes in pattern that can be identified in a data set and attributed to a geological formation or structure (Qureshi and Hinze 1989;

Himabindu and Ramdass, 2003; Adiri et al., 2017). Lineaments provide the pathways for groundwater movement and are hydrogeologically very important (Sankar et al. 1996).

Based on the interpretation of satellite imagery a number of lineament sets traversing NNE-SSW have been identified and presented in the Fig.3. Apart from these, large numbers of prominent joints traversing E-W direction and other sets in NW-SE, WNW-ESE and NNW-SSE directions are clearly shown in the figure 3. The signatures of these lineament sets are not clear from the satellite image in the city area. It is expected that many of these joint sets continue in same direction in the city area below the ground surface.

~~A preliminary examination of the remote sensing image reveals a linear feature and suggests the presence of various lineaments (Himabindu and Ramdass, 2003; Qureshi and Hinze, 1989; Adiri et al., 2017). A number of lineament sets are mapped.~~ The major lineaments are passing through the Kailana Lake-Tahkt Sagar and the general trend is in E-W directions. The Kailana Lake-Takht Sagar and other water bodies, hills and ridges are interconnected through the set of these lineaments. Several lineaments that cross in the NW-SE, WNW-ESE, and NNW-SSE directions are shown in Figure 3. ~~The signatures of the southern portion of the lineaments cannot be easily seen in the satellite imagery due to urbanization activity in the city~~. As a result, these lineaments have an impact on water flow and provide seepage zones.

4.2 Relief Map

Relief and hypsometry (frequency distribution of elevations) data are analysed and delineate the maximum relief (390 m) that occurs near the Kailana Lake-Takht Sagar and structural hills (in purple) shown in relief on the map (Fig. 4). The study area is highly undulating in nature. High relief areas are characterised by the rhyolite hills near Kailana Lake–Takht Sagar, while low relief areas are covered by quaternary deposits in the city. The relief map shows that elevations drop approximately 30 m in the water seepage area (a problematic area) in comparison to the Kailana Lake-Takht Sagar area. A gradual decline in the elevation from upstream to downstream is seen in the south and north-east directions on the relief map. The variations in elevation are between 390 m and 107 m in the study area.

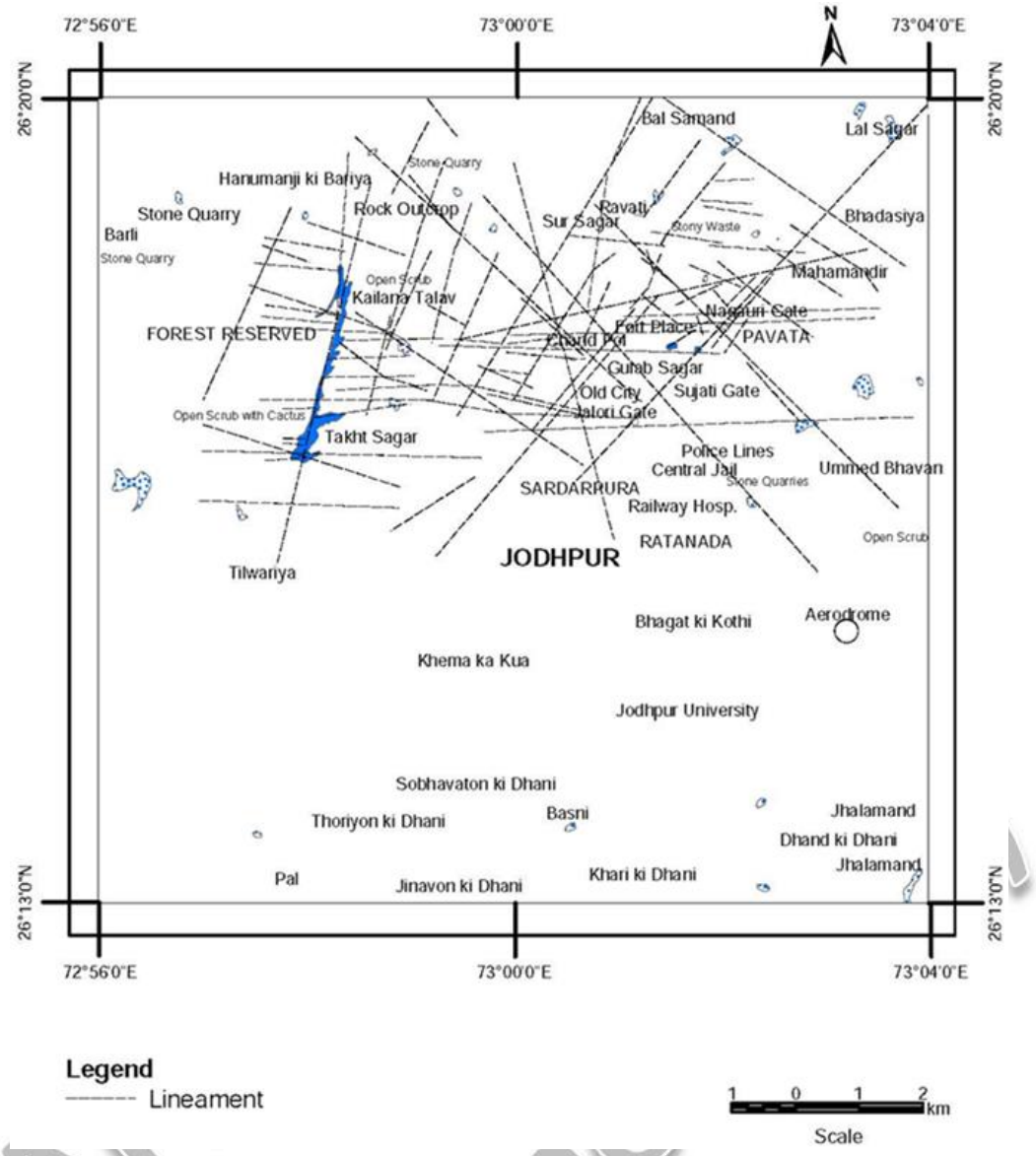

Figure 3. Lineament map inferred from ETM satellite image, showing the existence of lineaments and their interconnectivity

4.3. Geoelectrical Sounding (GS)

The studies of the geo-electrical sounding curves used both quantitative and qualitative methods. The interpreted geoelectrical sounding results are shown in Table 1. The VES curve obtained in the study area showed H, HA, HK, KH, QH, and HKH types. The interpreted VES results revealed three to five subsurface geo-electric layers delineated as surface soil, dry sand and kankar, shale, sandstone, fractured rhyolite, and compact rhyolite basement. The surface soils have apparent resistivity, which ranged from 23 to 780 ohm-m and depth ranges from 1.0 to 7.0 m, showed that they were made up of wind-blown sandy soil mixed with sand. Due to the various soil characteristics and varying levels of dryness and moisture, the surface soil resistivity values vary

from place to place. Due to the high sand content of the surface soil, which acts as a transmission medium for groundwater flow, and the presence of weathered and fractured formations, which influence groundwater circulation in the study area.

Table 1 Interpreted results of geoelectrical soundings in terms of thickness and resistivity

Sounding No.	Layer 1		Layer 2		Layer 3		Layer 4		Layer 5	
	ρ_1 (Ω-m)	h_1 (m)	ρ_2 (Ω-m)	h_2 (m)	ρ_3 (Ω-m)	h_3 (m)	ρ_4 (Ω-m)	h_4 (m)	ρ_5 (Ω-m)	h_5 (m)
(1)	(2)	(3)	(4)	(5)	(6)	(7)	(8)	(9)	(10)	(11)
1	378	3.8	248	7.8	50	50.0	∞	-	-	-
2	395	2.5	203	43.7	110	33.0	∞	-	-	-
3	409	1.0	220	36.6	125	29.0	∞	-	-	-
4	86	1.0	129	14.0	26	61.5	1160	-	-	-
5	200	1.3	250	4.6	46	17.4	28	-	-	-
6	120	1.2	180	4.8	17	34.0	85	-	-	-
7	110	1.9	220	1.8	70	11.8	14	28.9	∞	-
8	115	1.7	173	3.3	48	23.0	10	28.0	301	-
9	130	1.0	20	6.0	18	66.0	190	-	-	-
10	780	1.5	90	21.0	15	44.0	450	-	-	-
11	90	1.6	180	17.6	26	100.0	600	-	-	-
12	520	2.0	208	13.6	21	75.0	960	-	-	-
13	140	3.0	210	12.0	14	35.2	200	-	-	-
14	370	2.3	111	28.0	29	38.0	250	-	-	-
15	56	3.0	120	6.6	46	60.9	11	26.5	50	-
16	150	1.6	225	6.7	44	42.0	182	-	-	-
17	120	2.2	185	6.6	34	72.0	170	-	-	-
18	95	1.7	190	15.6	27	60.0	∞	-	-	-
19	130	1.8	41	10.8	24	18.0	72	-	-	-
20	170	1.2	110	14.4	680	-	-	-	-	-
21	300	2.0	450	8.0	15	10.0	300	-	-	-
22	125	1.6	36	12.3	25	19.0	85	-	-	-
23	76	2.1	112	4.4	17	36.0	∞	-	-	-
24	100	1.6	67	5.8	8	52.0	∞	-	-	-
25	60	2.0	18	5.4	6	40.0	23	-	-	-
26	160	2.0	104	8.2	11	46.0	47	-	-	-
27	62	1.6	42	25.6	11	-	-	-	-	-
28	23	1.2	12	9.6	23	-	-	-	-	-
29	84	1.4	299	4.2	60	9.7	24	87.0	98	-
30	52	2.1	130	11.3	22	98.0	88	-	-	-
31	103	5.1	18	106.5	77	-	-	-	-	-
32	170	1.4	68	6.1	91	26.2	14	63.8	9	-
33	172	1.3	215	2.3	63	14.4	10	-	-	-
34	45	2.0	157	7.2	18	71.1	300	-	-	-
35	31	1.6	103	3.6	14	20.0	∞	-	-	-
36	120	2.0	40	8.0	10	50.8	1200	-	-	-
37	298	3.5	123	9.6	14	38.4	∞	-	-	-
38	55	1.0	165	8.0	30	20.0	150	-	-	-
39	36	1.8	108	12.8	31	87.5	102	31.5	156	-
40	50	1.4	150	7.0	36	5.0	13	42.0	192	-
41	54	1.3	162	3.9	60	22.5	21	56.5	330	-
42	275	2.4	54	19.8	16	50.0	288	-	-	-
43	103	4.5	68	9.0	38	6.0	19	58.0	344	-
44	54	7.0	36	14.0	14	42.0	126	-	-	-
45	40	2.0	120	4.0	34	18.0	12	48.0	∞	-

46	90	6.8	36	20.4	96	2.7	47	26.4	4202	-
47	280	3.2	93	9.6	34	36.0	1050	-	-	-
48	110	3.0	106	2.0	140	7.9	125	20.0	500	-
49	400	5.4	80	42.0	240	-	-	-	-	-
50	340	1.1	113	4.4	65	5.2	126	-	-	-
51	100	3.0	67	6.0	117	4.3	60	16.0	180	-
52	134	3.1	5	5.9	237	-	-	-	-	-
53	122	1.6	13	19.0	763	-	-	-	-	-
54	62	1.0	93	4.0	30	11.0	15	56.0	31	-
55	74	1.0	111	2.0	33	16.4	13	62.0	38	-
56	130	1.0	260	2,0	70	5.2	26	20.0	180	-
57	180	1.7	90	10.2	26	40.0	250	-	-	-
58	170	2.0	85	26.0	24	54.0	210	-	-	-
59	150	3.6	75	40.0	190	-	-	-	-	-
60	40	2.0	20	6.0	13	48.0	∞	-	-	-
61	48	1.4	72	11.2	7	72.0	660	-	-	-
62	42	1.5	68	10.9	12	34.0	37	26.0	∞	-
63	30	1.4	3	8.4	11	84.0	38	-	-	-
64	50	1.8	70	6.5	14	21.9	∞	-	-	-
65	85	1.2	38	4.4	57	10.5	28	42.0	127	-
66	50	1.8	63	14.0	25	38.0	∞	-	-	-
67	421	3.0	96	16.0	21	24.0	150	-	-	-
68	140	4.0	120	12.0	20	46.0	∞	-	-	-
69	140	2.0	93	32.0	10	3.6	∞	-	-	-
70	200	1.4	20	22.4	400	-	-	-	-	-
71	160	1.0	380	4.0	22	150.0	990	∞	-	-

With the use of lithological data that may be accessed from the boreholes and geo-electrical characteristics generated from the interpretation of geo-electrical soundings. For the purpose of measuring the lateral and vertical extents of cracked zones, seven vertical subsurface geo-electrical cross-sections were created. These sections provide a good picture of fractured zones and underlying geological formations and delineate the subsurface formations that serve as conduits for groundwater seepage. For the sake of simplicity, the geo-electrical sections in Jodhpur City that passed through the seepage and the surrounding area have only been presented.

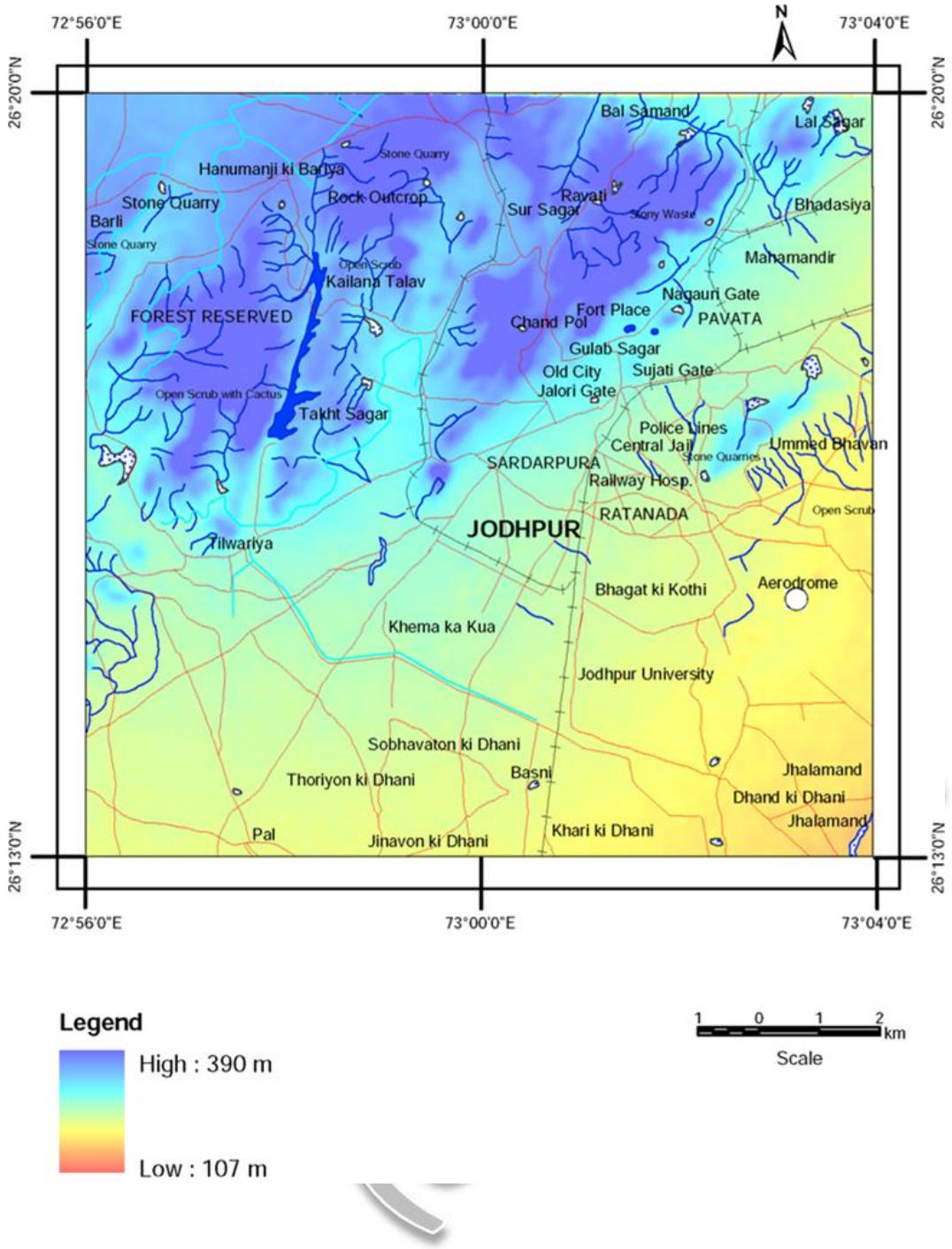

Figure 4. Relief map inferred from ETM satellite image, showing elevation distributions

4.4 Subsurface geoelectrical cross-section along profile A-A'

The subsurface geo-electrical cross-section was created using the lithology data from the boreholes BH-50, H-47, and piezometer (P/Z-1), as well as the outcomes of GS-1, GS-2/3, GS-66, GS-65, and GS-64. This cross-section has a length of around 8 kilometres overall and is oriented from WNW to ESE. This section indicated the existence of four geo-electrical layer formations, while at GS-65, there are five geo-electrical layer

formations (Figure 5). These are the surface soil, dry sand and kankar, shale, sandstone, semi-fractured rhyolite, fractured rhyolite, and compact rhyolite basements. The first layer, which is top-surface soil, has a resistivity range of 50 to 395 ohm-m and a thickness range of 1 to 3 m. Underlying the topsoil is a mixed formation of semi-fractured rhyolite with a resistivity value of 203 ohm-m on the western side and dry sand mixed with kankar on the eastern side with a resistivity range of between 57 and 70 ohm-m and a thickness range of between 6 and 42 m. The third layer is composed of fractured rhyolite in GS-1, GS2/3, P/Z-, and BH-50, while GS-64, GS-65, GS-66, and BH-47 are shale formations. The resistivity of this layer ranges between 110 and 14 ohm-m, while the thickness ranges between 20 and 80 m. The fifth layer encountered at GS-65 is a sandstone with a resistivity of 127 ohm-m and a thickness of approximately 5 m. The last layer is made up of a compact rhyolite basement that is extremely resistive and extends from 60 m onward. The area of seepage is traversed by the westernmost segment of the section due to the presence of semi-fractured to fractured rhyolite.

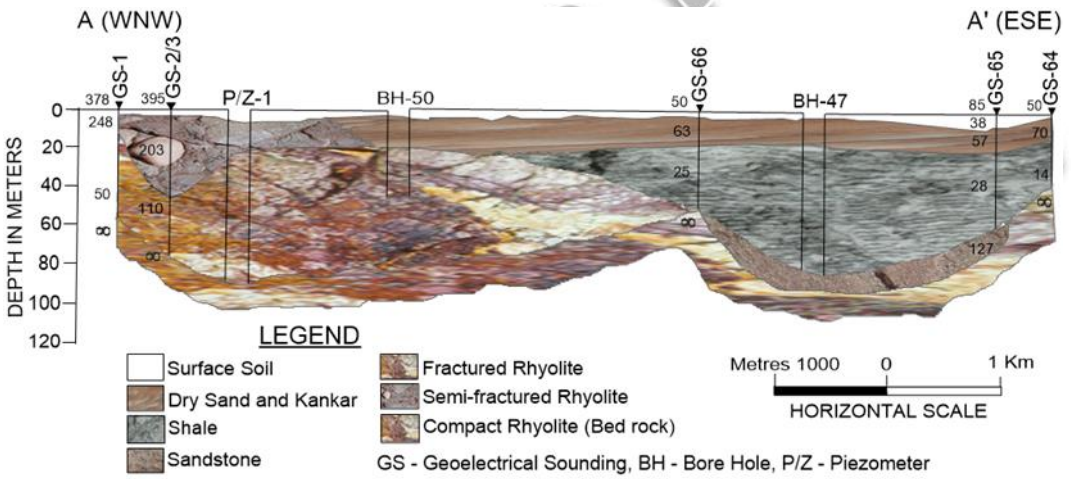

Figure 5. Subsurface geoelectrical cross section along profile A-A'

4.5 Subsurface geoelectrical cross-section along profile B-B'

The subsurface geoelectrical section shown in Figure 6 was created using the data from the existing boreholes BH-5, BH-23, BH-45, and BH-46 as well as the results of GS-48, GS-59, GS-58, GS-66, GS-67, and GS-68. This cross-section also passes through the seepage zone and is oriented WSW-ENE. The resistivity of the surface soil ranged from 42-170 ohm-m and the thickness from 1-4 m. The variations in the resistivity values of the surface soil are due to the different compositions of the soil. The second geoelectrical layer is characterised

by resistivity values from 63 to 160 ohm-m and a thickness of 3 to 40 m. It consists mainly of sand and kankar due to its thick sandy contents, which serve as the permeable medium for groundwater seepage. The third geo-electrical layer consists of a mixed formation of fractured rhyolite encountered at GS-48, GS-59, GS-58, BH-5 and BH-23 on the westerly side, having resistivity 40-210 ohm-m and thickness 10-30 m, which supports the groundwater seepage. The GS-59, GS-58, GS-66, GS-67 and GS-68 revealed the shale formation has resistivity ranges of 20-24 ohm-m with varying thickness. An isolated patch of semi-fractured and sandstone was encountered at GS-48 and GS-67. The compact rhyolite basement at a depth beyond 80 m exists. There is a possibility that groundwater will leak from the western side of the section upper part because it is composed of sandy, fractured and semi-fractured rhyolite formations.

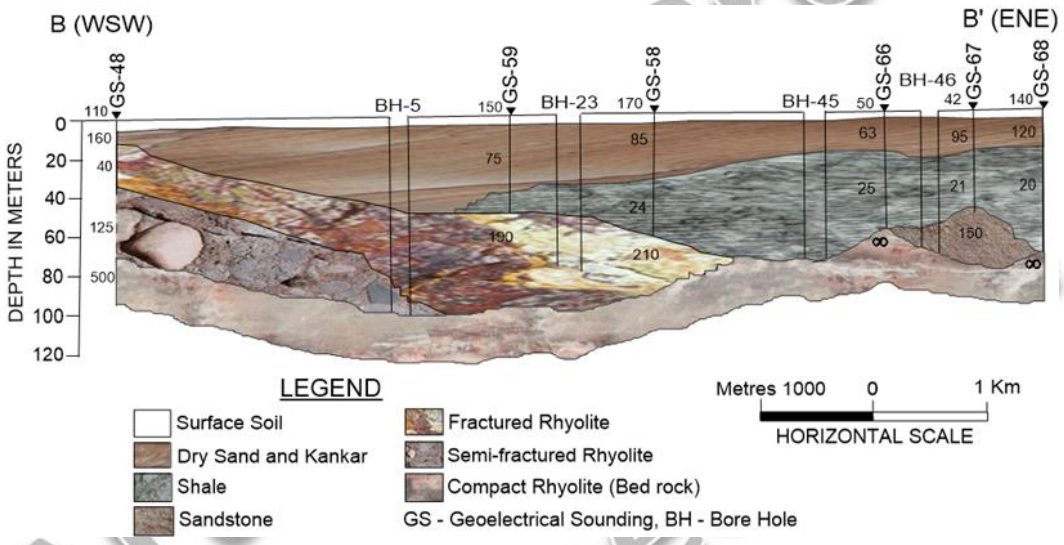

Figure 6. Subsurface geoelectrical cross-section along profile B-B'

4.6 Subsurface geoelectrical cross-section along profile E-E'

The results of quantitative interpretation of four geoelectrical soundings (GS-2/3, GS-48, GS-8, and GS-14) were correlated with records of existing piezometers and boreholes (P/Z-2, BH-43, and BH-33) to prepare this section. Figure 7 shows the resistivity values of the various formations observed in the study area, as well as their thickness and depth from the top surface. This cross-section has a length of 7.4 km and is oriented in the NNE-SSW direction. There are four layers of stratification visible across the geo-electric cross-section. The section depicts the first layer, which is made up of surface soil with resistivity values ranging from

110 to 395 ohm-m and a thickness 1 to 5 m. The second layer is composed of semi-fractured rhyolite with a resistivity of 203 ohm-m on the northern side and a sandy layer with varying resistivity values of 40 to 111 ohm-m on the southern side. The thickness of the second layer varies from 4 to 20 m. The third geo-electrical layer in this series is made up of fractured rhyolite on the northern side with a resistivity of 110–125 ohm–m and a thick layer of shale between BH–43 and GS–14 on the southern side with a resistivity of 10-29 ohm–m. Near the middle of the passage, both formations are squeezed out. The lingering presence of a semi-fractured zone and bedrock on the section's northern side are represented by the final layer. This semi-fractured zone may contribute to groundwater seepage.

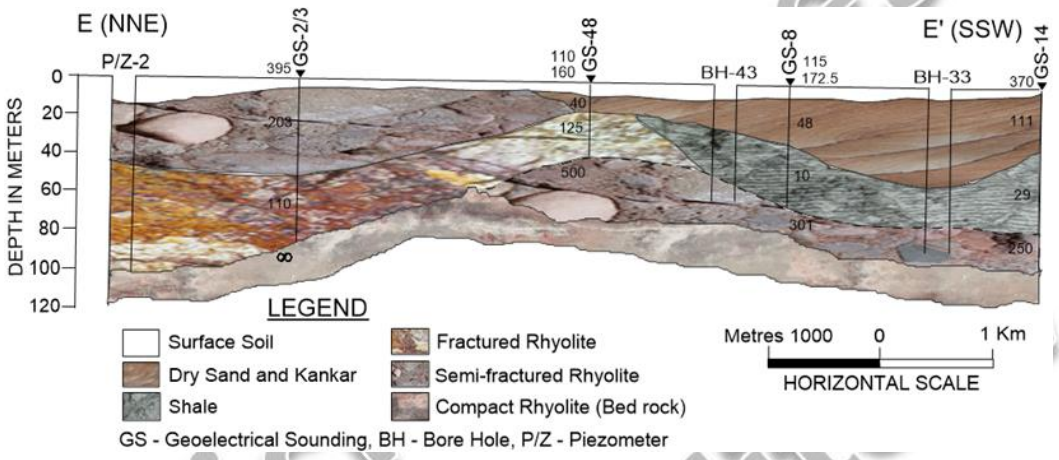

Figure 7. Subsurface geo-electrical cross-section along profile E-E'

4.7 Subsurface geoelectrical cross-section along profile F-F'

The section also covers a major part of the seepage region. The cross-section runs in the NE-SW direction and incorporates the results of GS-69, GS-66, GS-62, GS-57, and GS-45. Figure 8 was correlated with the lithological formation records of existing boreholes BH-1, BH-53, and BH-44. This cross-section consists of five geo-electrical layers and covers 8.8 km in length. The section displays the surface soil top layer with resistivity values of 40 to 180 ohm-m and a thickness of 1 to 6 metres. The second layer is made up of dry sand and kankar with different thicknesses of 8 to 32 m, and its resistivity ranges from 34 to 93 ohm-m. Except for the central area, where sandstone of resistivity 26 ohm-m and on the northern and southern sides shale with resistivity values 10-12 ohm-m are present throughout this section. This stratum has a thickness range of 2 to 20 metres. The isolated patch of semi-fractured rhyolite with a resistivity of 150 ohm-m is present at GS-57 in the

middle of the cross section. The last geo-electrical layer is composed of compact rhyolite on the northern side and granite on the southern side of the section. The presence of sedimentary formations of sand, sandstone, and a patch of semi-fractured rhyolite supports the groundwater seepage.

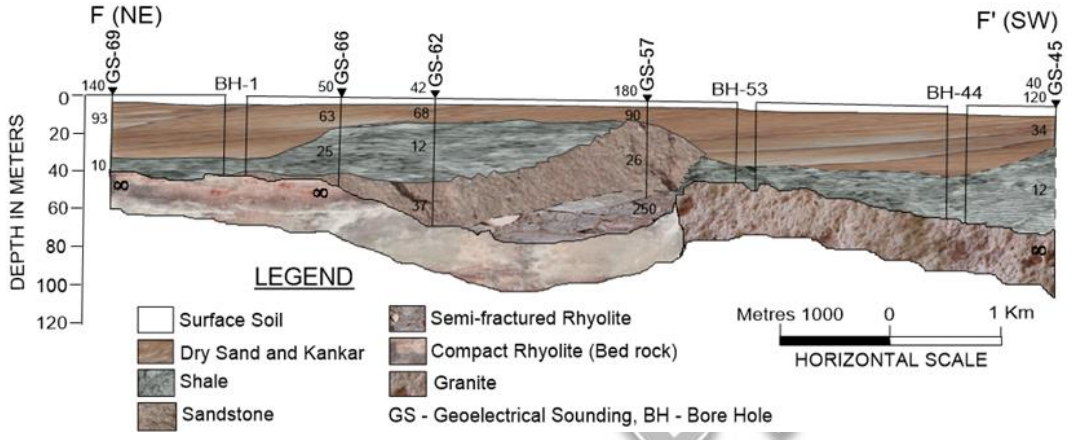

Figure 8. Subsurface geoelectrical cross-section along profile F-F'

Conclusions

In this study, geo-electrical resistivity techniques were combined with a rapid, cost-effective remote sensing methodology to map structural features, faults, and fracture zones that are favourable to water seepage. The interpretation of satellite imagery reveals a number of minor and major lineament sets have been mapped and traversed in E-W, NW-SE, WNW-ESE, and NNW-SSE directions. The majority of the lineaments are interconnected and pass through Kailana Lake-Takht Sagar. These lineaments provide easy conduits for the water seepage in the area. The elevation drops throughout the study area play a crucial role in enhancing the water seepage. The geo-electrical cross-section delineates sandy, semi-fractured, and fractured formations from the upper layer to greater depths in the region. Semi-fractured formations are frequently found immediately beneath the top soil layer, which penetrates down to a greater depth. In the study region, the interconnection of several major lineament sets and fractured zones through Kailana Lake-Takht Sagar was exposed to be a significant contributor to water seepage, according to the analysis of integrated data.

Acknowledgments

The author is thankful to the Department of Geophysics, Banaras Hindu University, Varanasi, for providing the necessary facilities to carry out this work. I am also grateful to the previous Head of the Geophysics wing (Dr. S. M. Pandey), GWD, Jodhpur, Rajasthan, for providing all the required facilities during the collection of data and fieldwork.

References

Abidin, M.H.Z., Baharuddin M.F.T., Zawawi M.H., Md Ali N, Madun A., Tajudin S.A.A. (2015). Groundwater Seepage Mapping using Electrical Resistivity Imaging. Applied Mechanics and Materials 773-774, 1524-1534. doi:10.4028/www.scientific.net/AMM.773-774.1524.

Adiri, Z., El-Harti, A., Jellouli, A., Lhissou, R., Maacha, L., Zouhair, M., Bachoui, E. (2017). Comparison of Landsat-8, ASTER and Sentinel-1 satellite remote sensing data in Automatic Lineaments Extraction: a case study of Sidi Flah-Bouskour inlier, Moroccan Anti Atlas. Adv Space Res 60, 2355–2367.

Al-Djazouli, M.O., Elmorabiti, K., Rahimi, A., Amellah, O., Fadil, O.A.M. (2020). Delineating of groundwater potential zones based on remote sensing, GIS and analytical hierarchical process: a case of Waddai,eastern Chad. GeoJournal: 1–14. https://doi.org/10.1007/s10708-020-10160-0.

Al-Fares, W. (2011). Contribution of the Geophysical methods in characterizing the water leakage in Afamia B dam, Syria. Journal of Applied Geophysics 75, 464-471.

Al-Fares, W. (2014). Application of Electrical Resistivity Tomography Technique for Characterizing Leakage Problem in Abu Baara Earth Dam, Syria. International Journal of Geophysics (14), 1-9. http://dx.doi.org/10.1155/2014/368128.

Al-Fares, W. (2019). Characterization of the leakage problem in Salhab earthen dam using electrical resistivity tomography and SP measurements, Syria. Contributions to Geophysics and Geodesy (49/4), 441-458 doi: 10.2478/congeo-2019-0023.

Ali, E.A., El-Khidir, S.O., Babikir, I.A.A., Abd El-Rahman, E.M. (2012). Landsat ETM+7 digital image processing techniques for lithological and structural lineament enhancement: case study around Abidiya area, Sudan. Remote Sens J 5, 83–89.

Bahuguna, I.M., Nayak, S., Tamilarsan, V., Moses, J. (2003). Groundwater prospective zone in basaltic terrain using remote sensing. Jour. Indian Soc. Remote Sensing 31(2), 102-105.

Bera, A., Mukhopadhyay, B.P., Barua, S. (2020). Delineation of groundwater potential zones in Karha river basin, Maharashtra, India, using AHP and geospatial techniques. Arabian Journal of Geosciences 13, 693. https://doi.org/10.1007/s12517-020-05702-2.

Bhattacharya, S., Das, S., Das, S., Kalashetty, M., Warghat, S.R. (2020). An integrated approach for mapping groundwater potential applying geospatial and MIF techniques in the semiarid region. Environ Dev Sustain: 1–6. https://doi.org/10.1007/s10668-020-00593-5.

Blanford, W.T. (1877). Geological notes on the Great Indian Desert between Sind and Rajasthan.Rec. Geol. Surv. India 10(1):1-54.

Chandrasekharan, H. (1988) Geoelectrical investigation for groundwater in Thar Desert Western Rajasthan; Some case studies. Trans. Istd. 12, 155-168.

Chandrasekharan, H., Navada, S.V. (2002). Interconnection between water bodies in the selected area of Rajasthan. In. Proceeding of the International Groundwater Conference (eds.) Thangrajan, M., Rai, S. N. and Singh V.S.) Oxford & IBH Pub Co Pvt. Ltd, New Delhi. 183-191.

Chopra, R.P.S. (1989). A temporal study of water logging in canal command area using remote sensing techniques. Journal of Applied Hydrology 11(2), 29-37.

Dailey, D., Saucka, W., Sultana, M., Milewskib, A., Ahmeda, M., Latond, W.R., Elkadiria, R., Fosterd, J., Schmidta, C., Al Harbia, T. (2015). Geophysical, remote sensing, GIS, and isotopic applications for a better

understanding of the structural controls on groundwater flow in the Mojave Desert, California. Journal of Hydrology: Regional Studies 3, 211-232.

Dar, I.A., Sankar, K., Dar, M.A. (2010). Remote sensing technology and geographic information system modeling: an integrated approach towards the mapping of groundwater potential zones in Hard rock terrain, Mamundiyar basin. J Hydrol 394, 285–295.

Das, S. (2017). Delineation of groundwater potential zone in hard rock terrain in Gangajalghati block, Bankura district, India using remote sensing and GIS techniques. Model Earth Syst Environ 3(4), 1589–1599. https://doi.org/10.1007/s40808-017-0396-7.

Denne, J.E., Yarger, H.L., Macfarlane, P.A., Knapp, R.W., Sophocleous, M.A., Lucas, J.R., Steeples, D.W. (1984). Remote sensing and geophysical investigation of glacial buried valleys in Northestern Kansas. Ground Water 22(1), 56-65.

Ebert, A. (1943). Grundlagen Zur Auswerkung geoelectrischer Tiefenmessungon, Gerlands Beitrage Zur Geopysik, BZ 10(1), 1-17.

Elbeih, S.F. (2014). An overview of integrated remote sensing and GIS for groundwater mapping in Egypt. Ain Shams Eng J 6(1), 1–15. https://doi.org/10.1016/j.asej.2014.08.008.

Elmahdi, S.I., Mohamed, M.M. (2014). Relationship between geological structures and groundwater flow and groundwater salinity in Al-Jaaw plain, United Arab Emirates, mapping and analysis by means of remote sensing and GIS. Arab J Geosci 7, 1249–1259.

Engelbert, P.J., Hotchkiss, R.H., Kelly, W.E. (1997). Integrated remote sensing and geophysical techniques for locating canal seepage in Nebraska. Journal of Applied Geophysics 38(2), 143-154. DOI: 10.1016/S0926-9851(97)00022-0.

Ghose, B. (1965). The genesis of the desert plains in central Luni basin of western Rajasthan. Jour. Indian Soc. Soil Sci. 13(2), 123-126.

Ghose, B., Singh, S. (1975). Geomarphology of prior and present drainage networks and their control on groundwater in sandstone formations, Jodhpur district, Annual report, CAZRI, Jodhpur.

Guo, Y., Cui, Y.A., Xie, J., Luo, Y., Zhang, P., Liu, H., Liu, J. (2022). Seepage detection in earth-filled dam from self-potential and electrical resistivity tomography. Engineering Geology 306, 106750 https://doi.org/10.1016/j.enggeo.2022.106750.

Gupta, A.K., Sharma, J.R., Bothale, R.V., Dharmavat, R., Singh, P. (2007). Jodhpur the gateway of India desert-study on rising ground water levels in the city. IGS News 13, 42-52.

Hamimi, Z., Hagag, W., Kamh, S., El-Araby, A. (2020). Application of remote-sensing techniques in geological and structural mapping of Atalla Shear Zone and Environs, Central Eastern Desert, Egypt. Arabian Journal of Geosciences 13, 414. https://doi.org/10.1007/s12517-020-05324-8.

Himabindu, D., Ramadass, G. (2003). Structural inferences from satellite image in and around Gadag, in the Dharwar Craton. Jour. Indian Soc. Remote Sensing. 31(3), 219-225.

Huang, Y., Fipps, G., Mass, S.J., Flecher, R.S. (2009). Airborne remote sensing for detection of irrigation canal leakage. Irrig. and Drain. Published online in Wiely Inter Science DOI:10.102/ird.511.

Isiorho, S.A., Nkereuwem. (1996). Reconnaissance study of the relationship between liniments and fractures in the southwest portion of the Lake Chad Basin. Journal of Environment & Engineering Geophysics 1(1), 47-54. https://doi.org/10:4133/JEEG.1.47.

Javed, A., Wani, M.H. (2009). Delineation of Groundwater Potential Zones in Kakund Watershed, Eastern Rajasthan, Using Remote Sensing and GIS Techniques. Journal of the Geological Society of India 73(2), 229-236.

Jigyasa, S. (2011). Seasonal variation in ground water quality of Jodhpur city and surrounding areas. Res. J. Chem. Environ. 5, 883–888.

Kansoh, R., Abd-El-Mooty, M., Abd-El-Baky, R. (2020). Computing the Water Budget Components for Lakes by Using Meteorological Data. Civil Engineering Journal 6(7), 1255-1265. http://dx.doi.org/10.28991/cej-2020-03091545.

Kar, A. (1986). Remote sensing of buried former streams in the extremely arid terrain of Jaisalmer, Indian desert for water and salinity. Proc. 7th Asian Remote Sensing Conference Oct. 23, 228.

Kar, A., Ghosh, B. (1984). The Drisavati river system of India an assessment and new findings. The Geographical Jour. 150, 221-229.

Kaur, L., Ramanathan, A.L. (2016). Assessment of Major Ion Chemistry in Ground Water and Surface Water of Kailana Lake Area of Jodhpur (Rajasthan). Jo WREM 3(2):42-56.

Khan, M.A., Mohrana, P.C. (2002). Use of remote sensing and Geographical Information System in the delineation and characterization of groundwater prospect zones. Jour. Indian Soc. Remote Sensing 30(3), 131-141 DOI:10.1007/BF02990645.

Kumar, R., Pal, S.K., Gupta, P.K. (2021). Water Seepage Mapping in an Underground Coal-Mine Barrier Using Self-potential and Electrical Resistivity Tomography. Mine Water and the Environment https://doi.org/10.1007/s10230-021-00788-w.

Machiwal, D., Jha, M.K., Mal, B.C. (2011). Assessment of groundwater potential in a semi-arid region of India using remote sensing, GIS and MCDM techniques. Water Resour Manag 25(5), 1359–1386. https://doi.org/10.1007/s11269-010-9749-y.

Mageshkumar, P., Subbaiyan, A., Lakshmanan, E., Thirumoorthy, P. (2019). Application of geospatial techniques in delineating groundwater potential zones: a case study from South India. Arabian Journal of Geosciences 12, 151 https://doi.org/10.1007/s12517-019-4289-0.

Manap, M.A., Nampak, H., Pradhan, B., Lee, S., Sulaiman, W.N.A., Ramli, M.F. (2014). Application of probabilistic-based frequency ratio model in groundwater potential mapping using remote sensing data and GIS. Arab J Geosci 7, 711–724.

Minsley, B.J., Burton, B.L., Ikard, S., Powers, M.H. (2011). Hydrogeophysical Investigations at Hidden Dam, Raymond, California. Journal of Environmental & Engineering Geophysics 16(4), 145-164 DOI: 10.2113/JEEG16.4.145.

Mshiu, E.E. (2011). Landsat Remote Sensing data as an alternative approach for geological mapping in Tanzania: a case study in the rung we volcanic province, south-western Tanzania. Tanz J Sci 37, 26–36.

Mulder, V.L., de Bruin, S., Schaepman, M.E., Mayr, T.R. (2011). The use of remote sensing in soil and terrain mapping – a review. Geoderma 162, 1–19.

Nejad, S.G., Falah, F., Daneshfar, M., Haghizadeh, A., Rahmati, O. (2017). Delineation of groundwater potential zones using remote sensing and GIS-based data-driven models. Geocarto International 32(2), 167–187. http://dx.doi.org/10.1080/10106049.2015.1132481.

Olasunkanmi, N.K., Aina, A., Olatunji, S., Bawala, M. (2018). Seepage investigation on an existing dam using integrated geophysical methods. Journal of Environment and Earth Science 8(5), 6-16,

Paliwal, B.S. (1992). Tectonics of the post-Aravalli mountain building activity and its bearing on the accumulation of sediments along the western flank of the Aravalli range, Rajathan, India.In:R. Ahmed and A.M.Sheikh, (eds.), Geology in the South Asia-I Proc. of GEOSAS-I Islamabad, Pakistan, Feb. 23-27, Hydrocarban Development Institute of Pakistan, 52-60.

Paliwal, B.S., & Rathore, P.S. (2000). Neoproterozoic volcanics and sedimentaries of Jodhpur: A reappraisal. In: Gyani, K.C., and Kataria, P. (Eds.), Proc. National Seminar "Tectonomagmatism, Geochemistry and Metamorphism of Precambrian Terrains", University Department of Geology, Udaipur, pp.75-94.

Pathak, S., Bhadra, B.K., Sharma, J.R. (2012). Study of influence of effluent on ground water using remote sensing, GIS and modelling techniques. International Archives of the Photogrammetry, Remote Sensing and Spatial Information Sciences, Volume XXXIX-B4, XXII ISPRS Congress, 25 August -1 September 2012, Melbourne, Australia.

Pratap, B., Raju, N.J., Yadav G.S. (2014). Investigation of seepage channel using remote sensing technique in Jodhpur City Rajasthan. https://link.springer.com/book/10.10072F978-3-319-18663-4.

Pratap, B., Yadav, G.S. (2016). Delineation of Ground water bearing fracture zone using VLF-EM methods in parts of Jodhpur City Rajasthan, India. Jour. of Applied Hydrology XXIX (1-4), 01-08.

Qureshi, M.N., Hinze, W.J. (1989). Workshop Overview Proc.Joint Indo-U.S. workshop on regional geophysical lineaments.Their tectonic and economic significances, Mem. Geol. Soc. India. Banglore 12, 3-10.

Rai, B., Tiwari, A., Dubey, V.S. (2005). Identification of groundwater prospective zones by using remote sensing and geoelectrical methods in Jharia and Raniganj coalfields, Dhanbad district, Jharkhand state. J. Earth Syst. Sci. 114(5), 515–522.

Rajput, S., Kumar, D., Ahmed, S. (2006). Delineation of groundwater prospect zones in hard rocks using remote sensing and GIS - A case study from Rajasthan. Journal of the Geological Society of India 68(2), 259-268.

Raju, R.S., Raju, G.S., Rajasekhar, M. (2019). Identification of groundwater potential zones in Mandavi River basin, Andhra Pradesh, India using remote sensing, GIS and MIF techniques. HydroResearch 2, 1–11.

Rao, D.P. (1995). Remote sensing for earth resources. A.E.G. publication.

Rao, D.P. (2000). Applications of space technology in groundwater studies. Bhu-Jal News 15(1&2), 24-29.

Rijkstwaterstaat, (1969). Standard graphs for resistivity prospecting. EAEG, Netherlands.

Sahai, B., Bhattacharya, A., Hegde, V.S. (1991). IRS-1A Application for Groundwater Targeting. Current Science 61 (3&4), 172-179.

Shankarnarayan, K.A., Chatterji, P.C., Singh, S. (1983). Role of remote sensing in ground water extraction for problem villages and habitants of hard rock regions of western Rajasthan. Proc. 2nd all India Conf. Drilling Equipment for groundwater extraction, New Delhi, 1/3 -1/25.

Sharafi, M., Khatami (2013). Detection of high local groundwater inflow to rock tunnels using ASTER satellite images. International Archives of the Photogrammetry, Remote Sensing and Spatial Information Sciences, Volume XL-1/W3, SMRP 2013, 5-8 October 2013, Tehran, Iran.

Shekhar, S., Pandey, A.C. (2015). Delineation of groundwater potential zone in hard rock terrain of India using remote sensing, geographical information system (GIS) and analytic hierarchy process (AHP) techniques. Geocarto Int. 30, 402–421.

Shukla, J.P., Pandey, S.M. (1991). Suitability of electrical resistivity survey for selecting ancient site in order to augment groundwater-A case study. Annals of Arid Zone 30(3), 187-195.

Singh, A.K., Prakash, S.R. (2002). An integrated approach of remote sensing, geophysics and GIS to evaluation of groundwater potentiality of Ojhala sub watershed, Mirzapur District, U.P. India. https://www.GISdevelopment.net.

Sinha, U.K., Kulkarni, K.M., Sharma, S., Ray, A., Bodhankar, N. (2002). Assessment of aquifer systems using isotope techniques in urban centres Raipur, Calcutta and Jodhpur, India. IAEA-TECDOC-1298, 77–94.

Srivastava, P.K., Bhattacharya, A.K. (2006). Groundwater assessment through an integrated approach using remote sensing, GIS and resistivity techniques: a case study from a hard rock terrain. Int J Remote Sens 27(20), 4599–4620.

Srivastava, V.K., Giri, D.N., Bharadwaj, P. (2012). Study and Mapping of Ground Water Prospect using Remote Sensing, GIS and Geoelectrical resistivity techniques – a case study of Dhanbad district, Jharkhand, India. J. Ind. Geophys Union 16 (2), 55-63.

Suganthi, S., Elango, L., Subramanian, S.K. (2013). Groundwater potential zonation by Remote Sensing and GIS techniques and its relation to the Groundwater level in the Coastal part of the Arani and Koratalai River Basin, Southern India. Earth Sci. Res. SJ. 17(2), 87-95.

Tagnon, B.Q., Assoma, V.T., Mangoua, J.M.O., Douagui, A.G., Savané, I. (2018). Contribution of SAR/RADARSAT-1 and ASAR/ENVISAT images to geological structural mapping and assessment of lineaments density in Divo-Oume area (Côte d'Ivoire). Egypt J Remote Sens Space Sci. https://doi.org/10.1016/j.ejrs.2018.12.001.

Takorabt, M., Toubal, A.C., Haddoum, H., Siham Zerrouk, S. (2018). Determining the role of lineaments in underground hydrodynamics using Landsat 7 ETM+ data, case of the Chott El Gharbi Basin (western Algeria). Arabian Journal of Geosciences 11: 76. https://doi.org/10.1007/s12517-018-3412-y.

Techerepanov, E.N., Zolatrik, V.A. (2002) Application of remote sensing for hydrological studies in the Nebraska sand hills in G.S.A. abstract with program, Denver, Colorado, Oct. 27-31, p. 88.

Yadav, G.S., Abolfazli, H. (1998). Geoelectrical soundings and their relationship to hydraulic parameters in semiarid regions of Jalore, Northwestern India. Jour. Appl. Geoph. 39: 35-51.

Yadav, G.S., Pandey, S.M., Kumar Niraj. (2000). Geoelectrical soundings for locating fresh groundwater zones around Jhanwar area of Jodhpur district. Proc. National Seminar GWR-98, Dept. of Geophysics, B.H.U. 93-98.

Yadav, G.S., Pratap, B. (2015). Identification of Responsible Source for Rise in Ground water Table of Jodhpur City, Rajasthan, India. Int. J. Earthquake Engg. Geol Sci. 5(1), 1–14.